Target Localization and Tracking for an Isogradient Sound Speed Profile

Hamid Ramezani, Hadi Jamali-Rad, *Student Member, IEEE*, and Geert Leus, *Fellow, IEEE*

***Abstract*—In an underwater medium the sound speed is not constant, but varies with depth. This phenomenon upsets the linear dependency of the distance traveled by an acoustic wave to the time it takes for the wave to travel that distance, and therefore makes existing distance-based localization algorithms less effective in an underwater environment. This paper addresses the problems of localizing a fixed node and tracking a mobile target from acoustic time-of-flight (ToF) measurements in a three-dimensional underwater environment with an isogradient sound speed profile. To solve these problems we first analytically relate the acoustic wave ToF between two nodes to their positions. After obtaining sufficient ToF measurements, we then adopt the Gauss-Newton algorithm to localize the fixed node in an iterative manner, and we utilize the extended Kalman filter for tracking the mobile target in a recursive manner. Through several simulations, we will illustrate that the proposed algorithms perform superb since they meet the Cramér-Rao bound (CRB) for localization and posterior CRB for tracking.**

***Index Terms*—Extended Kalman filter, Gauss-Newton algorithm, localization, ray tracing, sound speed profile, tracking, underwater acoustic sensor networks.**

I. Introduction

A wide variety of applications including early warning systems for natural disasters (e.g., tsunamis), ecosystem monitoring, oil drilling and military surveillance are the main driving force behind exploring underwater environments [1]. Recent advances in the design of wireless sensor networks (WSNs) motivated system designers to exploit underwater acoustic sensor networks (UASNs) for data gathering and ocean explorations. In order to interpret the sensed data in a meaningful manner, we require the sensor positions either remotely or locally as in terrestrial WSNs. Very low bit rate, low link quality, multi-path, time variability, and a depth-dependent sound speed profile (SSP) are the most important characteristics that make underwater acoustic communications a challenging field of research [2]. The aforementioned challenging characteristics, therefore, necessitate the design and development of new localization and tracking algorithms.

A complete survey of techniques and challenges in underwater localization can be found in [3], [4]. In [5], the authors propose a centralized algorithm to overcome the severe multipath property of the underwater environment due to scattering from the seabed and ocean surface. In [6], a time-difference-of-arrival-based localization scheme for stationary UASNs is proposed which does not require time synchronization among network nodes. In [7], depth information as well as range measurements are used to localize a target node inside a three-dimensional (3-D) area.

As stated before, one of the underwater localization challenges is the depth-dependent SSP which varies with temperature, pressure, and salinity [8]. Due to this property, an acoustic ray does not propagate along a straight line, but it bends. Even if the nodes are located at the same depth, the distance between the two nodes in an underwater environment is not linearly proportional to the wave travel time. However, in all the above mentioned underwater localization schemes, the propagation sound speed is assumed constant, and thus the trajectory of the ray will be a straight line. This assumption is unrealistic in general and degrades the performance of underwater localization algorithms.

In contrast to the aforementioned algorithms, [9] evaluates the localization performance degradation of the straight-line propagation model compared to the real propagation model. As the target node measures the time-of-flight (ToF) from an anchor node, the corresponding constant range interval surface for this measured ToF is constructed. To construct such a constant range interval surface (or a curve in a 2-D medium), the path trajectory for each departing ray from the considered anchor node is calculated. Then, on each path trajectory a point is selected related to the ToF. All these points together yield the desired constant range interval surface. After sufficient ToF measurements are collected, the position of the target is estimated as the point whose sum of squared distances from all these surfaces is minimum. The main drawback of this approach is the computational complexity which depends on the network size and the required accuracy. In [10], it is stated that in an underwater medium with an isogradient SSP the path trajectory becomes an arc of a circle. Nonetheless, non-straight-line wave propagation is neglected in [10]. Since the recovery of missing links is the main goal of [10], the positioning error is basically dominated by the error due to missing links. The authors of [11] consider a real wave propagation model for UASNs localization based on the depth information and SSP. They eliminate

Manuscript received October 03, 2011; revised May 08, 2012; revised May 08, 2012 and November 02, 2012; accepted November 04, 2012. Date of publication December 19, 2012; date of current version February 25, 2013. The associate editor coordinating the review of this manuscript and approving it for publication was Prof. Andrea Cavallaro. This work was supported by the European Commission FP7-ICT Cognitive Systems, Interaction, and Robotics under the Contract 270180 (NOPTILUS). Part of this work was presented at the Proceedings of the IEEE International Conference on Communications (ICC2012), June 2012.

The authors are with the Faculty of Electrical Engineering, Mathematics and Computer Science, Delft University of Technology, 2826 CD Delft, The Netherlands (e-mail: h.mashhadiramezani@tudelft.nl; h.jamalirad@tudelft.nl; g.j.t.leus@tudelft.nl).

Color versions of one or more of the figures in this paper are available online at http://ieeexplore.ieee.org.

Digital Object Identifier 10.1109/TSP.2012.2235432

the underwater range computation by using a look up table (LUT), which relates the travel time information to the horizontal distance between two nodes. Their proposed algorithm is very fast, but to scan the whole environment a huge LUT is required which may not be practical. Furthermore, the SSP in an underwater medium is subject to changes in temperature and conductivity, and any change in SSP degrades the LUT accuracy and therefore affects the localization performance. Finally, [12] considers the problem of ranging in an underwater environment. In that paper, a numerical range estimator is proposed which is based on reconstructing the slanted path using Fermat's principle and calculus of variations. Basically, after depth and time measurements are taken, an integral equality is formed which is taken over the depth between the nodes. Then, the constant defined by Snell's law is numerically calculated, which is used to compute the horizontal distance between the nodes through another integral equality. The work of [12] is really comprehensive, since with any given SSP, the horizontal distance is computable. However, the algorithm may compute the constant (defined by Snell's law) with an ambiguity, since in an underwater medium it is common that a traveling ray from one node to another passes a given depth more than once. As the depth of a node on a traveling ray is not a monotonic function of the depth, this phenomenon yields an ambiguous value for any integral taken with respect to (w.r.t.) the depth along the traveling path.

In this work, we propose a UASN localization and tracking approach for an underwater medium with an isogradient SSP. The isogradient SSP is a good assumption for deep water environments [13], [14], since the conductivity and water temperature in a deep underwater medium are constant, and the only factor that affects the SSP is the pressure which linearly depends on the depth. Notably, the measured SSP in a deep underwater medium is more accurate than the measured SSP in shallow waters [15]. In order to find the location of a target, we analytically relate the position of that node to the ToFs. Using at least four ToF measurements from four anchors, we formulate the localization problem. It will be shown that the ToF measurements in an underwater medium are a non-linear function of the target position, and consequently the localization problem is categorized as a non-linear least squares problem. The analytical relationship between the ToFs and the nodes' positions also allows us to compute the derivatives of the ToFs with respect to the target's position in closed form, and hence enables us to utilize efficient methods to solve the non-linear least squares localization problem, such as the Gauss-Newton method, the Levenberg-Marquardt method, the Powell's Dog Leg method, and so on. The Gauss-Newton algorithm (GNA) is the basis of many efficient methods for solving non-linear least squares problems, and in this paper we use this algorithm for estimating the target's position. In addition, since tracking is also important, we perform multilateration recursively by using the extended Kalman filter (EKF). Although other tracking methods could be adopted, we select the EKF because of the availability of the derivative of the measurements w.r.t. the location variables.

We do not require any depth information in our algorithms, and we directly work with ToF measurements based on a given SSP. However, since some autonomous acoustic vehicles are equipped with pressure sensors [14], [16], we also investigate the existence of depth information in our algorithms. To the best of our knowledge, this is the first work that analytically solves the problem of accurate localization and tracking in an isogradient SSP underwater environment with only ToF binformation.

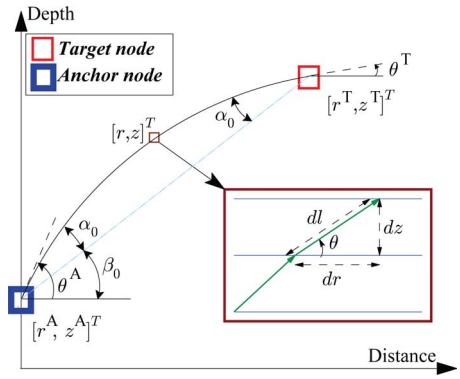

Fig. 1. Description of a ray between a target node and an anchor node.

The rest of the paper is organized as follows. In Section II, we analyze the characteristics of a ray traveling between two points, and also explain how the positions of the two nodes are related to the ToF. In Section III, the static localization algorithm is introduced, and its corresponding Cramér-Rao bound (CRB) is derived. We analyze the problem of mobile target tracking in Section IV, where we calculate the posterior CRB (PCRB). We evaluate the performance of the proposed algorithms in Section V through several simulations, and finally conclude the paper in Section VI.

II. Ray Tracing Between Two Points

We consider the problem of tracing a ray between two nodes, e.g., A (anchor) and T (target), in a 3-D environment with an isogradient sound speed where the SSP is only dependent on the depth, and has the following form

$$C(z) = b + az, \tag{1}$$

where z denotes the depth, b indicates the sound speed at the surface, and a is a constant depending on the environment. Without loss of generality, to solve the ray tracing problem between the two nodes, we assume that the z axis crosses node A. Therefore, due to the cylindrical symmetry around the z axis we can transfer the ray tracing problem to the plane which includes both nodes and the z axis as shown in Fig. 1. In this figure, $r^{\mathrm{T}} - r^{\mathrm{A}}$ represents the horizontal distance between the nodes, and it can be written as

$$r^{\mathrm{T}} - r^{\mathrm{A}} = \sqrt{(x^{\mathrm{T}} - x^{\mathrm{A}})^2 + (y^{\mathrm{T}} - y^{\mathrm{A}})^2}, \tag{2}$$

where $x^{\mathrm{T}}, y^{\mathrm{T}}, x^{\mathrm{A}}$, and y^{A} indicate the x-coordinate and y-coordinate of respectively point T and point A in a 3-D environment. Since the z-axis is assumed to cross point A, we actually have $r^A = 0$ but we keep it in our formulation for representation purposes.

Acoustic propagation is usually modeled using a ray tracing approach which is a valid approximation for the aforementioned isogradient SSP underwater environment. Ray tracing is guided by Snell's law given by [11]

$$\frac{\cos\theta}{C(z)} = \frac{\cos\theta^{\mathrm{A}}}{C(z^{\mathrm{A}})} = \frac{\cos\theta^{\mathrm{T}}}{C(z^{\mathrm{T}})} = k_0, \text{ and } \theta \in \left[\frac{-\pi}{2}, \frac{\pi}{2}\right], \quad (3)$$

where θ^{T} and θ^{A} are the ray angles at the target node and anchor node locations, respectively, as illustrated in Fig. 1. z^{A} and z^{T} represent the depth of the anchor node and the target node, respectively, and k_0 is constant along a ray traveling between the nodes. Moreover, the parameters θ and z represent the angle and depth of a given point along the ray. From Fig. 1, we can write

$$\partial r = \frac{\partial z}{\tan\theta}, \quad (4a)$$

$$\partial l = \frac{\partial z}{\sin\theta}, \quad (4b)$$

$$\partial t = \frac{\partial l}{C(z)}, \quad (4c)$$

where l is the arc length of a ray traveling between the two nodes, and t is its corresponding travel time. Moreover, using (1) and (3), and by taking derivatives w.r.t. z and θ, we can write

$$\partial z = -\frac{1}{ak_0}\sin\theta\,\partial\theta. \quad (5)$$

In the following subsections, we show how the above partial derivatives can be used for extracting the ray characteristics.

A. Time of Flight vs. Sensor Node Locations

In this part of the paper, it is shown how the ToF between the two nodes is related to their positions. By substituting (5) into (4a), and integrating w.r.t. θ we have

$$r^{\mathrm{T}} - r^{\mathrm{A}} = -\frac{1}{ak_0}\left(\sin\theta^{\mathrm{T}} - \sin\theta^{\mathrm{A}}\right), \quad (6)$$

for the horizontal distance, and for the vertical distance between the two nodes we can write

$$z^{\mathrm{T}} - z^{\mathrm{A}} = \frac{1}{ak_0}\left(\cos\theta^{\mathrm{T}} - \cos\theta^{\mathrm{A}}\right). \quad (7)$$

Dividing (7) by (6), considering $r^{\mathrm{T}} \neq r^{\mathrm{A}}$ we end up with

$$\frac{z^{\mathrm{T}} - z^{\mathrm{A}}}{r^{\mathrm{T}} - r^{\mathrm{A}}} = -\frac{\cos\theta^{\mathrm{T}} - \cos\theta^{\mathrm{A}}}{\sin\theta^{\mathrm{T}} - \sin\theta^{\mathrm{A}}}, \text{ for } r^{\mathrm{T}} \neq r^{\mathrm{A}}. \quad (8)$$

Furthermore, by substituting (1) into (3) we can write one more equality as

$$\frac{b + az^{\mathrm{T}}}{b + az^{\mathrm{A}}} = \frac{\cos\theta^{\mathrm{T}}}{\cos\theta^{\mathrm{A}}}. \quad (9)$$

By applying the change of variables $\theta^{\mathrm{A}} = \beta_0 + \alpha_0$, and $\theta^{\mathrm{T}} = \beta_0 - \alpha_0$, (8) and (9) can be modified to

$$\frac{z^{\mathrm{T}} - z^{\mathrm{A}}}{r^{\mathrm{T}} - r^{\mathrm{A}}} = \tan\beta_0, \text{ for } r^{\mathrm{T}} \neq r^{\mathrm{A}}, \quad (10)$$

$$\frac{b + az^{\mathrm{T}}}{b + az^{\mathrm{A}}} = \frac{1 - \tan\beta_0\tan\alpha_0}{1 + \tan\beta_0\tan\alpha_0}. \quad (11)$$

The parameter β_0 denotes the angle of the straight line between the two nodes w.r.t. the horizontal axis, and α_0 represents the angle at which the ray trajectory deviates from this straight line as shown in Fig. 1. For the exceptional condition where $z^{\mathrm{A}} = z^{\mathrm{T}}$, (11) is not informative and should be modified to

$$\tan\alpha_0 = \frac{1}{2}\frac{a(r^{\mathrm{T}} - r^{\mathrm{A}})}{b + az^{\mathrm{T}}}, \text{ for } z^{\mathrm{T}} = z^{\mathrm{A}}, \quad (12)$$

which is extracted from (6). Now, by integrating (4c) w.r.t. θ, the ToF can be calculated as

$$t = -\frac{1}{a}\left(\ln\frac{1 + \sin\theta^{\mathrm{T}}}{\cos\theta^{\mathrm{T}}} - \ln\frac{1 + \sin\theta^{\mathrm{A}}}{\cos\theta^{\mathrm{A}}}\right). \quad (13)$$

In the above equation for the special case where $r^{\mathrm{A}} = r^{\mathrm{T}}$, one node is located on top of the other node, and thus according to Snell's law we have $\theta = \pm\frac{\pi}{2}$, or $\partial s = \pm\partial z$. In this exceptional case, the ToF can be given by

$$t = \begin{cases} -\frac{1}{a}\ln\frac{C(z^{\mathrm{T}})}{C(z^{\mathrm{A}})} & \text{for } z^{\mathrm{T}} < z^{\mathrm{A}} \\ -\frac{1}{a}\ln\frac{C(z^{\mathrm{A}})}{C(z^{\mathrm{T}})} & \text{for } z^{\mathrm{T}} > z^{\mathrm{A}}. \end{cases} \quad (14)$$

Since the occurrence probability of one node being located on top of the other is zero, we ignore it in the rest of this paper.

Up to now, the ToF for an isogradient SSP can be computed using (13) by first calculating β_0 from (10), substituting it into (11) and computing α_0, and consequently θ^A and θ^T. Since we will adopt the GNA for the static localization and the EKF for tracking a mobile target, in addition to the ToF as a function of the node locations, we also need the derivatives of the ToF w.r.t. the target location. Here, we assume that point A represents a fixed anchor node and point T represents the target node which can be fixed or mobile. To derive $\frac{\partial t}{\partial r^{\mathrm{T}}}$ and $\frac{\partial t}{\partial z^{\mathrm{T}}}$ using (13) we take the following partial derivatives

$$\frac{\partial t}{\partial r^{\mathrm{T}}} = -\frac{1}{a}\left(\frac{1}{\cos\theta^{\mathrm{T}}}\frac{\partial\theta^{\mathrm{T}}}{\partial r^{\mathrm{T}}} - \frac{1}{\cos\theta^{\mathrm{A}}}\frac{\partial\theta^{\mathrm{A}}}{\partial r^{\mathrm{T}}}\right), \quad (15a)$$

$$\frac{\partial t}{\partial z^{\mathrm{T}}} = -\frac{1}{a}\left(\frac{1}{\cos\theta^{\mathrm{T}}}\frac{\partial\theta^{\mathrm{T}}}{\partial z^{\mathrm{T}}} - \frac{1}{\cos\theta^{\mathrm{A}}}\frac{\partial\theta^{\mathrm{A}}}{\partial z^{\mathrm{T}}}\right). \quad (15b)$$

The above equations depend on the partial derivatives of the ray angles at the target and anchor location. These partial derivatives can be computed from (8) and (9) as

$$\frac{\partial\theta^{\mathrm{T}}}{\partial r^{\mathrm{T}}} + \frac{\partial\theta^{\mathrm{A}}}{\partial r^{\mathrm{T}}} = -\frac{z^{\mathrm{T}} - z^{\mathrm{A}}}{\left(r^{\mathrm{T}} - r^{\mathrm{A}}\right)^2}\frac{\left(\sin\theta^{\mathrm{T}} - \sin\theta^{\mathrm{A}}\right)^2}{1 - \cos\left(\theta^{\mathrm{T}} - \theta^{\mathrm{A}}\right)}, \quad (16a)$$

$$\frac{\partial\theta^{\mathrm{T}}}{\partial r^{\mathrm{T}}} - \frac{b + az^{\mathrm{T}}}{b + az^{\mathrm{A}}}\frac{\sin\theta^{\mathrm{A}}}{\sin\theta^{\mathrm{T}}}\frac{\partial\theta^{\mathrm{A}}}{\partial r^{\mathrm{T}}} = 0, \quad (16b)$$

$$\frac{\partial\theta^{\mathrm{T}}}{\partial z^{\mathrm{T}}} + \frac{\partial\theta^{\mathrm{A}}}{\partial z^{\mathrm{T}}} = \frac{1}{r^{\mathrm{T}} - r^{\mathrm{A}}}\frac{\left(\sin\theta^{\mathrm{T}} - \sin\theta^{\mathrm{A}}\right)^2}{1 - \cos\left(\theta^{\mathrm{T}} - \theta^{\mathrm{A}}\right)}, \quad (17a)$$

$$\frac{\partial\theta^{\mathrm{T}}}{\partial z^{\mathrm{T}}} - \frac{b + az^{\mathrm{T}}}{b + az^{\mathrm{A}}}\frac{\sin\theta^{\mathrm{A}}}{\sin\theta^{\mathrm{T}}}\frac{\partial\theta^{\mathrm{A}}}{\partial z^{\mathrm{T}}} = -\frac{a}{b + az^{\mathrm{A}}}\frac{\cos\theta^{\mathrm{A}}}{\sin\theta^{\mathrm{T}}}, \quad (17b)$$

where (16a) and (17a) are calculated from (8), and (16b) and (17b) are derived from (9). Observe that (16) and (17) are linear in $\frac{\partial\theta^{\mathrm{T}}}{\partial z^{\mathrm{T}}}$, $\frac{\partial\theta^{\mathrm{A}}}{\partial z^{\mathrm{T}}}$, $\frac{\partial\theta^{\mathrm{T}}}{\partial r^{\mathrm{T}}}$, $\frac{\partial\theta^{\mathrm{A}}}{\partial r^{\mathrm{T}}}$, and can thus simply be solved in closed form. By computing these values for each anchor and substituting them into (15a) and (15b), we are able to compute the

derivative of all measured ToFs w.r.t. the target node position. Finally, $\frac{\partial t}{\partial x^{\mathrm{T}}}$ and $\frac{\partial t}{\partial y^{\mathrm{T}}}$ can be derived as

$$\frac{\partial t}{\partial x^{\mathrm{T}}} = \frac{\partial t}{\partial r^{\mathrm{T}}} \frac{x^{\mathrm{T}} - x^{\mathrm{A}}}{r^{\mathrm{T}} - r^{\mathrm{A}}}, \tag{18a}$$

$$\frac{\partial t}{\partial y^{\mathrm{T}}} = \frac{\partial t}{\partial r^{\mathrm{T}}} \frac{y^{\mathrm{T}} - y^{\mathrm{A}}}{r^{\mathrm{T}} - r^{\mathrm{A}}}. \tag{18b}$$

B. Traveled Ray Length

As stated before, in an underwater medium, the traveled ray length between two points is not the same as the distance between them. In the next section, we will see that the distance-dependent noise is related to the received signal power, and consequently to the ray length. The ray length in an underwater medium with an isogradient SSP can be easily obtained by substituting (5) into (4b), and taking an integral w.r.t. θ, leading to

$$l = -(az^{\mathrm{T}} + b)\frac{\theta^{\mathrm{T}} - \theta^{\mathrm{A}}}{a\cos\theta^{\mathrm{T}}}, \tag{19}$$

where l is the traveled ray length between the nodes A and T.

Further, we will observe later on that in order to extract a lower bound on the position estimation variance, the partial derivatives of the traveled ray length w.r.t. the target location are needed. Below, we compute the derivative of the ray length w.r.t. r^{T} and z^{T} as a function of $\frac{\partial\theta^{\mathrm{T}}}{\partial r^{\mathrm{T}}}$, $\frac{\partial\theta^{\mathrm{T}}}{\partial z^{\mathrm{T}}}$, $\frac{\partial\theta^{\mathrm{A}}}{\partial r^{\mathrm{T}}}$, $\frac{\partial\theta^{\mathrm{A}}}{\partial z^{\mathrm{T}}}$:

$$\frac{\partial l}{\partial r^{\mathrm{T}}} = -\frac{az^{\mathrm{T}} + b}{a\cos\theta^{\mathrm{T}}}\left[\left(1 + \left(\theta^{\mathrm{T}} - \theta^{\mathrm{A}}\right)\tan\theta^{\mathrm{T}}\right)\frac{\partial\theta^{\mathrm{T}}}{\partial r^{\mathrm{T}}} - \frac{\partial\theta^{\mathrm{A}}}{\partial r^{\mathrm{T}}}\right] \tag{20a}$$

$$\frac{\partial l}{\partial z^{\mathrm{T}}} = -\frac{az^{\mathrm{T}} + b}{a\cos\theta^{\mathrm{T}}}\left[\left(1 + \left(\theta^{\mathrm{T}} - \theta^{\mathrm{A}}\right)\tan\theta^{\mathrm{T}}\right)\frac{\partial\theta\ \mathrm{T}}{\partial z^{\mathrm{T}}} - \frac{\partial\theta^{\mathrm{A}}}{\partial z^{\mathrm{T}}}\right] - \frac{\theta^{\mathrm{T}} - \theta^{\mathrm{A}}}{\cos\theta^{\mathrm{T}}}, \tag{20b}$$

where $\frac{\partial l}{\partial x^{\mathrm{T}}}$ and $\frac{\partial l}{\partial y^{\mathrm{T}}}$ can simply be calculated from $\frac{\partial l}{\partial r^{\mathrm{T}}}$. The partial derivatives $\frac{\partial l}{\partial x^{\mathrm{T}}}$ and $\frac{\partial l}{\partial y^{\mathrm{T}}}$ can be obtained from $\frac{\partial l}{\partial r^{\mathrm{T}}}$ similar to the computation of the partial derivatives of the ToF w.r.t. x^{T} and y^{T}.

C. Ray Depth Overshoot

In practice, the SSP of the entire underwater medium cannot be considered isogradient. However, the SSP can be modeled as isogradient within a certain depth range. In other words, the ocean environment can be divided into several isogradient SSP layers with various thicknesses. For instance in [13], it is shown that the SSP of the Pacific ocean from a depth of 600 m to a depth of 5000 m can be estimated as isogradient.

In an underwater environment with an isogradient SSP, it is probable that the depth of a node along a given ray between two points, say A and T, exceeds the region $[z^{\mathrm{A}}, z^{\mathrm{T}}]$. The depth of a node along a given ray can be expressed as a function of the ray angle as

$$z(\theta) = \frac{1}{a}\left(\frac{\cos\theta}{k_0} - b\right), \tag{21}$$

where k_0 is a positive constant defined earlier in (3). It is obvious that $z(\theta)$ follows the behavior of $\cos\theta$, and its extremum occurs at the maximum of $\cos\theta$, i.e., $\theta = 0$, since when $a > 0$ the ray bends towards the deeper regions whereas when $a < 0$ the ray bends upwards, i.e., to smaller depths. In other words, the depth of a node on a ray exceeds the region $[z^{\mathrm{A}}, z^{\mathrm{T}}]$ if and only if the sign of the ray angle at the two points differs from each other. Thereby, when we have $\theta^{\mathrm{A}}\theta^{\mathrm{T}} < 0$, the value of the minimum or the maximum depth can be computed as

$$\begin{aligned}\max_{\theta} z(\theta) &= 1/a(1/k_0 - b) \text{ if } a > 0\\ \min_{\theta} z(\theta) &= 1/a(1/k_0 - b) \text{ if } a < 0.\end{aligned} \tag{22}$$

If the computed $\max_\theta z(\theta)$ or $\min_\theta z(\theta)$ lies within the boundaries of the isogradient SSP layer, then the formulas derived in the previous subsections are valid.

D. Range Approximation Using Depth Information

The underwater nodes can also be equipped with a pressure sensor, which allows them to estimate their depth. Using this depth information as well as (8) to (13), the target node can compute its horizontal distance from each anchor, and use the traditional range-based WSN localization algorithms to find its position [17]. However, due to the computational complexity, it is sometimes preferable to approximate the underwater medium as a homogeneous one. Below, we will show that if the depth of the two nodes is known, the underwater environment can be approximated as a homogeneous one using the assumption of a straight-line wave propagation. By adopting such an approximation, the computational complexity of the localization scheme decreases, but its accuracy degrades.

With the assumption of a straight-line wave propagation, the ToF between two points can be written as

$$t_{\mathrm{sl}} = \int_{z^{\mathrm{A}}}^{z^{\mathrm{T}}} \frac{1}{\sin(\beta_0)}\frac{dz}{C(z)} = -\frac{1}{a\sin(\beta_0)}\ln\left(\frac{v^{\mathrm{T}}}{v^{\mathrm{A}}}\right), \tag{23}$$

where β_0 is the angle of the straight line between the two nodes w.r.t. the horizontal axis, as defined in (8). Hence, the average sound speed is

$$\bar{v}_{\mathrm{sl}} = \frac{\|\mathbf{x}^{\mathrm{T}} - \mathbf{x}^{\mathrm{A}}\|}{t_{\mathrm{sl}}} = \frac{v^{\mathrm{T}} - v^{\mathrm{A}}}{\ln(\frac{v^{\mathrm{T}}}{v^{\mathrm{A}}})} \tag{24}$$

where $\|\mathbf{x}^{\mathrm{T}} - \mathbf{x}^{\mathrm{A}}\|$ is the distance between the two points which is related to the depth of the nodes as

$$\|\mathbf{x}^{\mathrm{T}} - \mathbf{x}^{\mathrm{A}}\| = \frac{z^{\mathrm{T}} - z^{\mathrm{A}}}{\sin\beta_0}. \tag{25}$$

It can be seen that the average sound speed, under this assumption, only depends on the sound speed at the depths where the nodes are located. Moreover, it can be shown that based on the depth information of the nodes, (24) is the best linear approximation of the sound speed in an isogradient SSP medium. Regardless of the availability of the depth information, the distance error originating from the assumption of a constant wave propagation speed can be acquired as

$$E_r = t\bar{v} - \|\mathbf{x}^{\mathrm{T}} - \mathbf{x}^{\mathrm{A}}\|, \tag{26}$$

where t is the actual ToF between the two nodes, and $\bar{v}$ is the assumed constant sound speed. This also holds for the case of

a straight line propagation based on availability of depth information, i.e., $\bar{v} = \bar{v}_{\rm sl}$.

III. Target Localization Based on Time of Flight Measurements

In this paper, we consider a single target node whose position will be determined by a number of anchor nodes. However, the extension to multiple target nodes is easy. Two scenarios for multiple target localization can be considered. In a first scenario, the anchor nodes are transmitters and the target nodes are receivers. Then, each target node can measure the ToFs to the anchors individually and estimate its position. In a second scenario, the target nodes are transmitters and the anchors are receivers. Under this condition, if the target nodes send the ranging signal simultaneously, then there would be lots of uncertainties and ambiguities for the localization algorithm. Nevertheless, if we assume that each target transmits its ranging signal while the others are silent (for instance as in a TDMA scheme), then there will be no ambiguity and the proposed algorithm can be extended to a multiple target scenario.

In real scenarios we may only know that the sound speed varies linearly with depth, $C(z) = az + b$, but we do not know the value of a and b. In addition, the characteristics of the environment may change slowly with time, due to the water temperature and salinity, and consequently the values of a and b may change. Since we know the anchor positions, we can estimate the value of a and b by a simple training phase. For instance, the i-th anchor transmits a signal to the j-th anchor who can then compute the ToF. Repeating this procedure for all combinations of two anchors, we have $N(N-1)/2$ ToF measurements, and based on (10), (11) and (13) we are able to estimate the values of a and b. In this way, the algorithm can cope with slow variations of the environment.

To be able to measure the ToFs between the target node and the anchors, the target node needs to be synchronized with the anchor nodes of the network. Quite contrary to terrestrial WSNs, synchronizing a UASN is a difficult task. Large propagation delays and possible node movements are two significant attributes that severely affect UASN synchronization [18]. To eliminate this problem, a ping-pong style scheme to measure the round-trip delay between the target node and each of the anchor nodes can be employed [19]. However, in this paper we assume that all the nodes are synchronized, and we only focus on the error that results from the assumption of a straight-line propagation.

A. Static Network Model

We consider a 3-D underwater wireless sensor network consisting of $N \geq 4$ anchor nodes with known locations and one fixed target node. The ToF measurements are assumed to be affected by Gaussian distributed noise as

$$\tilde{\mathbf{t}} = \mathbf{f}(\mathbf{x}) + \mathbf{v}, \tag{27}$$

where $\mathbf{f}(.) = [f_1(.), f_2(.), \ldots, f_N(.)]^T$ is a function relating the actual ToFs to the target location $\mathbf{x} = [x, y, z]^T$ (we omit the superscript T for simplicity), $\tilde{\mathbf{t}} = \left[\tilde{t}_1, \tilde{t}_2, \ldots, \tilde{t}_N\right]^T$ is a vector containing the ToF measurements between the target node and each of the anchor nodes, and $\mathbf{v}$ represents the measurement noise. We assume that the noise components are mutually independent, and hence the covariance matrix of the noise vector can be obtained as

$$\mathbf{R}_v = \mathrm{diag}\left(\sigma_1^2, \sigma_2^2, \ldots, \sigma_N^2\right), \tag{28}$$

where σ_n^2, for $n \in \{1, 2, \ldots, N\}$, is the noise variance of the ToF measurement based on the n-th anchor node. Since the measurement errors in the ToFs are mutually uncorrelated, the maximum likelihood (ML) solution for $\mathbf{x} = [x, y, z]^T$ will be given by

$$\arg\min_{\mathbf{x}} \|\mathbf{f}(\mathbf{x}) - \tilde{\mathbf{t}}\|^2. \tag{29}$$

B. Proposed Positioning Algorithm

The optimization problem in (29) is non-linear w.r.t. the variable $\mathbf{x}$, and therefore it is difficult to be solved analytically. Here, we adopt a numerical system solver such as the GNA. The algorithm starts with an initial point and improves the estimate recursively as stated in Algorithm 1.

Algorithm 1: Gauss-Newton Algorithm

Start with an initial location guess.
Set $k = 1$ and put a large value in E.
while $k \leq K$ and $E \geq \epsilon$ **do**
  Next state:
  $\mathbf{x}^{(k+1)} = \mathbf{x}^{(k)} -$
  $\left(\nabla\mathbf{f}(\mathbf{x}^{(k)})^T \nabla\mathbf{f}(\mathbf{x}^{(k)})\right)^{-1} \nabla\mathbf{f}(\mathbf{x}^{(k)})^T \left(\mathbf{f}(\mathbf{x}^{(k)}) - \tilde{\mathbf{t}}\right)$
  $E = \|\mathbf{x}^{(k+1)} - \mathbf{x}^{(k)}\|$
  $k = k + 1$
end while
$\hat{\mathbf{x}} = \mathbf{x}^{(k)}$

In this algorithm, $\nabla\mathbf{f}(\mathbf{x}^{(k)}) = \left[\frac{\partial f_1}{\partial \mathbf{x}}, \frac{\partial f_2}{\partial \mathbf{x}}, \ldots, \frac{\partial f_N}{\partial \mathbf{x}}\right]^T_{\mathbf{x}=\mathbf{x}^{(k)}}$ represents the gradient of the vector $\mathbf{f}$ w.r.t. the variable $\mathbf{x}$ at $\mathbf{x}^{(k)}$, where $\mathbf{x}^{(k)}$ is the estimate at the k-th iteration, which can be computed using (15) and (18), and $\frac{\partial f_i}{\partial \mathbf{x}} = \left[\frac{\partial f_i}{\partial x}, \frac{\partial f_i}{\partial y}, \frac{\partial f_i}{\partial z}\right]^T$ for $i = 1$ to N. Here, K and ϵ are the user-defined limits on the stopping criteria that determine when the algorithm exits the loop. The parameter K denotes the total number of iterations, which depends on the required precision. In general, only a small K is required, i.e., $K = 7$ or even less.

In terms of computational complexity, Algorithm 1 indicates that each iteration requires two simple matrix multiplications, namely one $(.)_{3\times N}$ by $(.)_{N\times 3}$ multiplication (i.e., roughly $9N$ floating operations) as well as one $(.)_{3\times 3}$ by $(.)_{3\times N}$ multiplication (again roughly $9N$ floating operations), and one 3×3 matrix inversion (i.e., 27 floating operations). Furthermore, we also have to compute the elements of one $N \times 3$ matrix, $\nabla\mathbf{f}(\mathbf{x}^{(.)})$, and one $N \times 1$ vector, $\mathbf{f}(\mathbf{x}^{(.)})$, which are of order N. This means that in total we have a complexity of order N for each iteration.

C. Cramér-Rao Bound

The Cramér Rao bound (CRB) expresses a lower bound on the variance of any unbiased estimator of a deterministic parameter. In this subsection, we derive two CRBs for two dif-

ferent noise characteristics; distance-independent noise (DIN), for which the variance of the measurement noise is independent of the distance between the nodes, and distance-dependent noise (DDN), for which the variance of the measurement noise depends on the traveled ray length between the nodes. DDN is more realistic compared to DIN, since the accuracy of ToF estimation is related to the received signal power, which itself is related to the traveled distance and transmit power. The Fisher information matrix (FIM) for a system affected by independent Gaussian noise can be computed as [20]

$$\mathbf{I}(\mathbf{x})_{i,j} = \frac{\partial \mathbf{f}}{\partial x_i}^T \mathbf{R}_v^{-1} \frac{\partial \mathbf{f}}{\partial x_j} + \frac{1}{2} \operatorname{tr}\left[\mathbf{R}_v^{-1} \frac{\partial \mathbf{R}_v}{\partial x_i} \mathbf{R}_v^{-1} \frac{\partial \mathbf{R}_v}{\partial x_j}\right], \tag{30}$$

where

$$\frac{\partial \mathbf{f}}{\partial x_i} = \left[\frac{\partial f_1}{\partial x_i}, \frac{\partial f_2}{\partial x_i}, \ldots, \frac{\partial f_N}{\partial x_i}\right]^T, \tag{31}$$

and

$$\frac{\partial \mathbf{R}_v}{\partial x_i} = \operatorname{diag}\left(\frac{\partial [\mathbf{R}_v]_{11}}{\partial x_i}, \frac{\partial [\mathbf{R}_v]_{22}}{\partial x_i}, \ldots, \frac{\partial [\mathbf{R}_v]_{NN}}{\partial x_i}\right), \tag{32}$$

and x_i is the i-th element of $\mathbf{x}$, i.e, $x_1 = x, x_2 = y$, and $x_3 = z$. Once the FIM is computed, the lower bound on the variance of the estimation error can be expressed as $\mathrm{CRB} = \sum_{i=1}^{3} \mathrm{CRB}_{x_i}$ where CRB_{x_i} is the variance of the estimation error in the i-th variable and it is defined as

$$\mathrm{CRB}_{x_i} = [\mathbf{I}^{-1}(\mathbf{x})]_{i,i}. \tag{33}$$

For DIN, the noise covariance matrix is fixed which means that the second term of the FIM in (30) is zero, and consequently the CRB computation can be simplified. On the other hand, for DDN, the noise covariance matrix depends on the distance traveled between each anchor and the target node according to

$$\sigma_n^2 = K_E A(l_n, f), \tag{34}$$

where K_E is a constant that is related to the transmission power and the environment noise floor, and $A(l_n, f)$ is the overall path loss, which can be defined as [21]

$$A(l_n, f) = \left(\frac{l_n}{l_0}\right)^{\beta} L(f)^{l_n - l_0}, \tag{35}$$

where f is the signal frequency, and l_n is the traveled distance which is taken in reference to some l_0. The path loss exponent β models the spreading loss, which is usually in between 1 and 2. The absorption coefficient $L(f)$ can be obtained using an empirical formula [21].

The computation of $\frac{[\partial \mathbf{R}_v]_{n,n}}{\partial x_i}$ in (32) requires the partial derivatives $\frac{\partial \sigma_n^2}{\partial x_i}$ for $i = 1, 2, 3$. The derivative of σ_n^2 w.r.t. the variable x_i, can be calculated as

$$\frac{\partial \sigma_n^2}{\partial x_i} = K_E \frac{l_n^{\beta-1}}{l_0^{\beta}} L(f)^{l_n - l_0} \left[\beta + l_n \ln L(f)\right] \frac{\partial l_n}{\partial x_i}, \tag{36}$$

which is related to the derivatives of the traveled ray length w.r.t. x_i. Once the above expressions are computed we are able to form $\frac{\partial \mathbf{R}_v}{\partial x_i}$ for each variable x_i, and based on that the FIM and consequently the CRB can be calculated.

D. Localization With Available Depth Measurements

The earlier localization algorithm does not require any depth information. In this subsection, we show how the optimization model will change if depth measurements are available. The result of this subsection is also useful for a comparison of the proposed algorithm with other existing state-of-the-art algorithms which mostly demand depth information. As stated in Section II-D, the underwater target can measure its depth with a pressure sensor, and may send this information to the central unit to potentially improve the localization accuracy. In this situation, the function $\mathbf{f}(\mathbf{x})$, the measurement vector, $\tilde{\mathbf{t}}$, and the covariance matrix of the noise vector, $\mathbf{R}_v$, have to be modified to the following format:

$$\mathbf{f}(.) = [f_1(.), f_2(.), \ldots, f_N(.), f_z(.)], \tag{37a}$$

$$\tilde{\mathbf{t}} = \left[\tilde{t}_1, \tilde{t}_2, \ldots, \tilde{t}_N, \tilde{z}\right]^T, \tag{37b}$$

$$\mathbf{R}_v = \operatorname{diag}\left(\sigma_1^2, \sigma_2^2, \ldots, \sigma_N^2, \sigma_z^2\right) \tag{37c}$$

where $f_z(\mathbf{x}) = z$, $\tilde{z}$ is the noisy depth measurement, and σ_z^2 is the power of the corresponding noise. Here, like the ToF measurements, it is assumed that the depth information is affected by Gaussian noise but does not generally depend on the distance from the anchors. As before, the ML solution for $\mathbf{x} = [x, y, z]^T$ is the same as (29). The GNA and CRB can be extended using (37).

IV. Target Tracking Based on Time of Flight Measurements

A. Dynamic Network Model

To be able to localize a mobile target in a recursive manner (sometimes referred to as tracking), we exploit the EKF to estimate and track the position. Let us denote the location of the mobile target at time instant k as $\mathbf{x}_k = [x_k, y_k, z_k]^T$, and the corresponding state vector for the EKF as $\mathbf{s}_k = [\mathbf{x}_k^T, \dot{\mathbf{x}}_k^T]^T$, which contains both the location and velocity of the mobile target at time instant k.

In general, a discrete-time linear movement process model can be considered as

$$\mathbf{s}_k = \mathbf{\Phi} \mathbf{s}_{k-1} + \mathbf{w}_k, \tag{38}$$

where the matrix $\mathbf{\Phi}$ relates the state of the previous time instant to the current one, and $\mathbf{w}_k$ represents an i.i.d. Gaussian process noise with covariance matrix $\mathbf{Q}_k$.

It is noteworthy that we can further improve the accuracy of our location estimate with the help of a depth measurement in cases where this information can be acquired. However, for the network to be able to exploit the depth of the mobile target, the node will have to transmit a signal containing the depth information to the anchors which itself is resource-demanding due to the bandwidth limitations of the underwater channel. In order to make this process more bandwidth efficient, we suppose that the mobile target transmits the depth information every ρ-th transmission frame. On the other hand, scenarios can be considered where the mobile target itself requires its location. Then, we can consider that depth information is always available. Although velocity measurements of the mobile target would aid the localization accuracy, in practice it requires the use of Doppler

sensors, which increases the implementation cost as well as the computational complexity, and hence, we avoid measuring the velocity. Thus, the measurement model under consideration can be described as

$$\tilde{\mathbf{t}}_k = \mathbf{h}(\mathbf{s}_k) + \mathbf{v}_k, \tag{39}$$

$$\tilde{z}_k = z_k + v_k \qquad \text{if} \quad \mathrm{mod}(k,\rho) = 0, \tag{40}$$

where $\mathbf{h}(.) = [h_1(.), h_2(.), \ldots, h_N(.)]^T$ is the function relating the state of the mobile target, $\mathbf{s}_k$ to the wave travel times between the mobile target and the N anchors, $\mathbf{t}_k = [t_{k,1}, \ldots, t_{k,N}]^T$ (note that $\mathbf{h}(\mathbf{s}_k) = \mathbf{f}(\mathbf{x}_k)$ from (27)). $\mathbf{v}_k$ and v_k represent the i.i.d. Gaussian noise of the measurements with covariance matrix $\sigma_t^2\mathbf{I}_N$ and variance σ_z^2, respectively, where $\mathbf{I}_N$ is the $N \times N$ identity matrix. In the following, we explain how we can utilize the EKF for localization and tracking of a mobile target in an underwater environment.

B. Extended Kalman Filter

The EKF algorithm for underwater tracking considering the exact SSP (EKF-ESSP) is shown in Algorithm 2. In this algorithm, $\mathbf{P}_k$, $\mathbf{R} = \sigma_t^2\mathbf{I}_N$, and $\mathbf{Q}_k$ are the covariance matrix of the error in the state estimate, the measurement noise, and the process noise, respectively. To linearize the measurement equations, we compute the gradient of $\mathbf{h}(.)$ as $\mathbf{H} = \nabla\mathbf{h}(\mathbf{s}) = \left[\frac{\partial h_1}{\partial \mathbf{s}}, \ldots, \frac{\partial h_N}{\partial \mathbf{s}}\right]^T$ where $\frac{\partial h_i}{\partial \mathbf{s}} = \left[\frac{\partial h_i}{\partial \mathbf{x}}^T, \frac{\partial h_i}{\partial \dot{\mathbf{x}}}^T\right]^T$, and $\frac{\partial h_i}{\partial \dot{\mathbf{x}}} = \mathbf{0}_{3\times 1}$ for $i = 1$ to N.

Algorithm 2: EKF

Start with an initial location guess.
for $k = 1$ to K **do**
  Next state:
    $\hat{\mathbf{s}}_k^- = \mathbf{\Phi}\hat{\mathbf{s}}_{k-1}$
  Next error covariance:
    $\mathbf{P}_k^- = \mathbf{\Phi}\mathbf{P}_{k-1}\mathbf{\Phi}^T + \mathbf{Q}_k$
  if z info. is not available : **then**
    Compute the Kalman gain:
      $\mathbf{K}_k = \mathbf{P}_k^-\mathbf{H}_k^T(\mathbf{H}_k\mathbf{P}_k^-\mathbf{H}_k^T + \mathbf{R})^{-1}$
    Update the state:
      $\hat{\mathbf{s}}_k = \hat{\mathbf{s}}_k^- + \mathbf{K}_k\big(\tilde{\mathbf{t}}_k - \mathbf{h}(\hat{\mathbf{s}}_k^-)\big)$
    Update the error covariance:
      $\mathbf{P}_k = (\mathbf{I} - \mathbf{K}_k\mathbf{H}_k)\mathbf{P}_k^-$
  else
    Compute the Kalman gain:
      $\breve{\mathbf{K}}_k = \mathbf{P}_k^-\breve{\mathbf{H}}_k^T(\breve{\mathbf{H}}_k\mathbf{P}_k^-\breve{\mathbf{H}}_k^T + \breve{\mathbf{R}})^{-1}$
    Update the state:
      $\hat{\mathbf{s}}_k = \hat{\mathbf{s}}_k^- + \breve{\mathbf{K}}_k\big([\tilde{\mathbf{t}}_k^T, \tilde{z}_k]^T - [\mathbf{h}(\hat{\mathbf{s}}_k^-)^T, \hat{z}_k^-]^T\big)$
    Update the error covariance:
      $\mathbf{P}_k = (\mathbf{I} - \breve{\mathbf{K}}_k\breve{\mathbf{H}}_k)\mathbf{P}_k^-$
  end if
end for

The gradient must be evaluated for time instant k as $\mathbf{H}_k = \nabla\mathbf{h}(\hat{\mathbf{s}}_k^-)$, where $\mathbf{h}(\hat{\mathbf{s}}_k^-)$ is the a posteriori location estimate at the k-th time instant. This matrix can again be computed using (15) and (18). Following the derivation of the EKF, if depth measurements are available, $\mathbf{H}_k$ and $\mathbf{R}$ should be modified to $\breve{\mathbf{H}}_k$ and $\breve{\mathbf{R}}$ as

$$\breve{\mathbf{H}}_k = \begin{bmatrix} \mathbf{H}_k \\ [0,0,1,0,0,0] \end{bmatrix},$$

$$\breve{\mathbf{R}} = \begin{bmatrix} \mathbf{R} & \mathbf{0}_{N\times 1} \\ \mathbf{0}_{N\times 1}^T & \sigma_z^2 \end{bmatrix} = \begin{bmatrix} \sigma_t^2\mathbf{I} & \mathbf{0}_{N\times 1} \\ \mathbf{0}_{N\times 1}^T & \sigma_z^2 \end{bmatrix},$$

where $\mathbf{0}_{m\times n}$ denotes an $m \times n$ all zero matrix.

C. Posterior Cramér-Rao Bound

The lower bound on the mean squared error (MSE) of estimation for any discrete-time filtering problem, like the proposed EKF, can be computed via the posterior Cramér-Rao bound (PCRB) [22]. The recursive PCRB derived in [23] provides a formula for updating the posterior FIM from one time instant to the next. The posterior FIM sequence $\mathbf{J}_k$ for a linear process and a non-linear measurement model can be computed as

$$\mathbf{J}_k = (\mathbf{Q}_k + \mathbf{\Phi}\mathbf{J}_{k-1}^{-1}\mathbf{\Phi}^T)^{-1} + \bar{\mathbf{H}}_k^T\mathbf{R}_k^{-1}\bar{\mathbf{H}}_k \tag{41}$$

where all the parameters have been defined earlier, except for $\bar{\mathbf{H}}_k$, which is the measurement gradient evaluated at the true location of the mobile target at the k-th time instant. It is noteworthy that, since we basically estimate the location of the mobile target and not its velocity, the PCRB of our location estimates will correspond to the sum of the first three diagonal elements of $\mathbf{J}_k^{-1}$

$$\mathrm{PCRB}_k = \sum_{i=1}^{3}\left[\mathbf{J}_k^{-1}\right]_{ii}. \tag{42}$$

Note that, the PCRB of the i-th element of $\mathbf{s}$ corresponds to the i-th diagonal element of $\mathbf{J}_k^{-1}$.

V. Numerical Results

In this section, we will conduct several simulations to evaluate the performance of our proposed algorithms in an environment with an isogradient SSP. We assume that the sound speed at the surface is $b = 1480$ m/s, and it increases as a linear function of depth with a steepness of $a = 0.1$. As a first simulation result, we compute the range error resulting from the straight-line wave propagation model with a constant velocity. This velocity can simply be assumed to be the sound speed at the anchor location or the target location, at the average depth between these two points, or the best linear approximation as given by (24). In Fig. 2, it is shown that as the target node gets further away from a surface anchor node, the error increases.

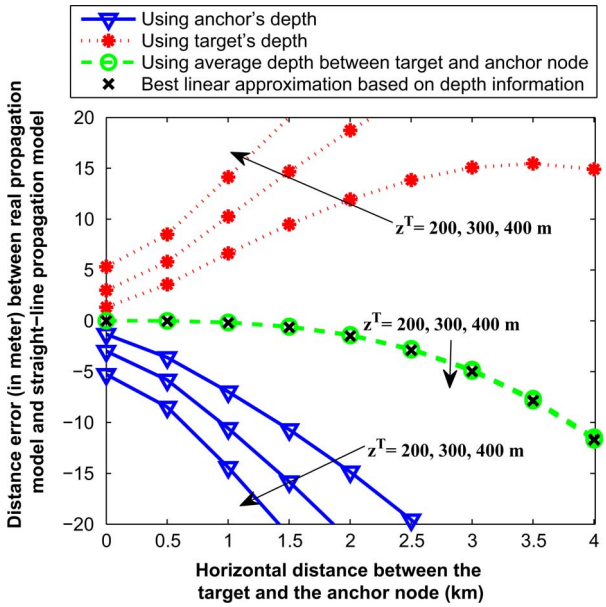

Fig. 2. Error in range calculation resulting from the assumption of a straight-line propagation with a constant speed.

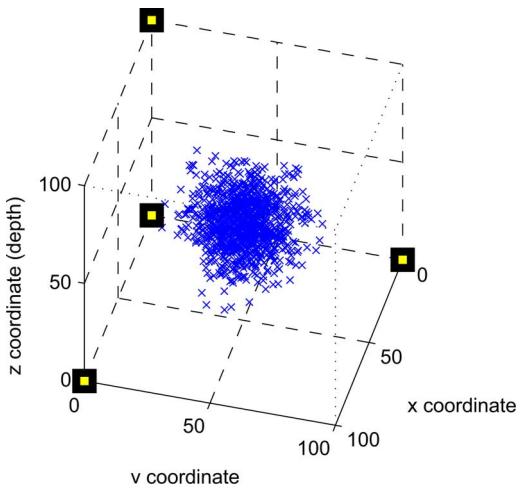

Fig. 3. Random target node position around the reference point (here the anchors' center of gravity).

Furthermore, it can be seen that among the different given constant speeds, the best linear approximation and the average one perform the best. However, these methods need the depth information of the target and anchor node which may not be available all the time.

At the network level, we consider four anchors that are located on the vertices of a cube with edge length 100 m, in which one vertex is located at the origin of the Cartesian coordinate system as depicted in Fig. 3. Here we consider the proposed localization algorithm (GNA-ESSP), and for the computation of each point in the following figures, we average the solution over 10^4 independent Monte Carlo runs. In addition, for the sake of comparison, we also consider an ordinary range-based localization algorithm which considers a constant sound speed defined as the average sound speed between two given nodes (GNA-ASSP)[1]. In the GNA-ASSP, the distance between two nodes is estimated via the measured ToFs, i.e., as $t\bar{v}$, where $\bar{v}$ is a given constant wave velocity. In our simulations, we simply take $\bar{v}$ as the average speed over the region where the deepest and the shallowest anchors are located. Hence, we simply set $\bar{v} = [C(\max_n z_n^{\mathrm{A}}) + C(\min_n z_n^{\mathrm{A}})]/2$. In each Monte Carlo run, the mobile target is located d meters away from a reference point in the 3-D environment, where d has a normal distribution with zero mean and standard deviation $10\sqrt{3}$ m. For instance, in Fig. 3, the reference point of the target location is set at the anchors' center of gravity, $[50, 50, 50]^T$, and for each Monte Carlo run the mobile target has a random position around this reference point. Note that we plot the mean CRB (for the localization scenarios) and mean PCRB (for the tracking scenarios) as we average over different realizations of target locations and trajectories, respectively.

Based on the target position, the actual ToFs between the target and the anchors are computed. These actual ToFs can be obtained either from the analytical formulas or by ray-tracing simulators [24]. In order to compute the ToFs via ray-tracing simulators, a bunch of rays with different angles (so that the whole area is scanned) departs the transmitter and the trajectories of all the rays are computed. Among all these rays we pick the ones which have two properties: first, they are close enough to the receiving point, and second, they arrive sooner than the other rays to the receiving point. Then, we restart the above procedure with another set of rays, but with a finer angular resolution. This time, the initial angles of these rays lay between the angles of the rays studied in the previous run. We continue this procedure until we get to the desired accuracy. Among the available simulators we have chosen the BELLHOP. The BELLHOP is a beam tracing model for predicting acoustic pressure fields in ocean environments and it can produce a variety of useful outputs including transmission loss, eigenrays, arrivals, and received time-series [25]. Notably, for the numerical results presented in this section, no reverberation due to scattering from fish or other biodata is considered.

After the ToF computation, noise is added to these ToFs and these noisy ToFs are used as an input to the considered localization algorithms. For our proposed GNA-ESSP the initial point is set to the anchors' center of gravity, and the stopping criteria are set to $K = 7$ and $\epsilon = 10^{-3}$.

In Fig. 4, we investigate the effect of the measurement noise on the algorithms under consideration. For this simulation, the reference point is located at the anchors' center of gravity, and the measurement noise variance for all measurements is considered to be the same and distance-independent. Here, the horizontal axis represents the noise standard deviation (std.) on the ToF measurements, and the vertical axis is the root mean squared error (RMSE) of the location estimate which is given by

$$\mathrm{RMSE} = \sqrt{\mathbb{E}\left[\|\hat{\mathbf{x}} - \mathbf{x}\|^2\right]}, \tag{43}$$

where $\mathbb{E}\{.\}$ represents the expectation operation.

[1]For the GNA-ASSP, the same GNA as in Algorithm 1 is used, but the gradient is computed according to the linear dependency of the ToF to the range in a homogeneous medium.

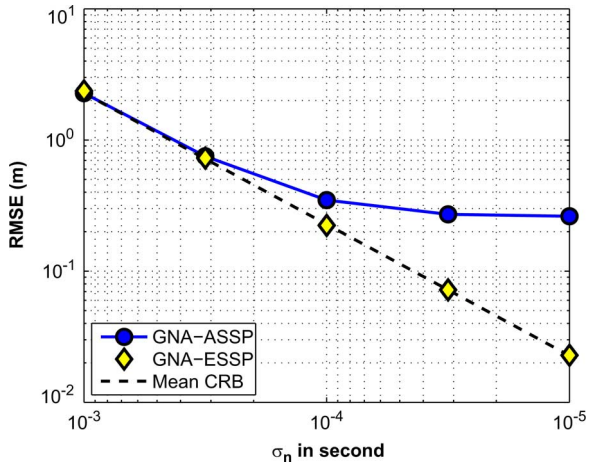

Fig. 4. Localization performance with distance-independent measurement noise.

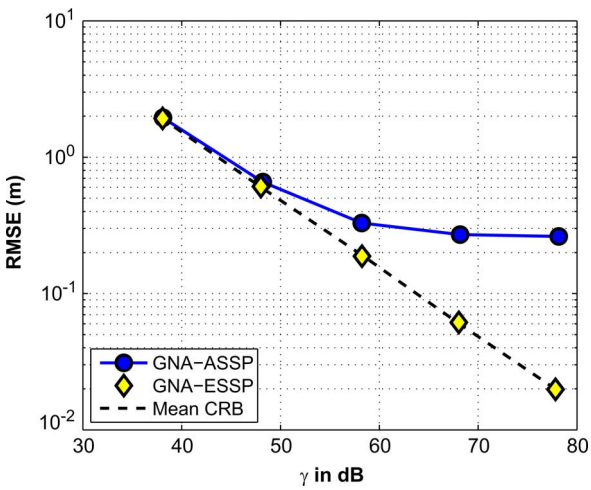

Fig. 5. Localization performance with distance-dependent measurement noise.

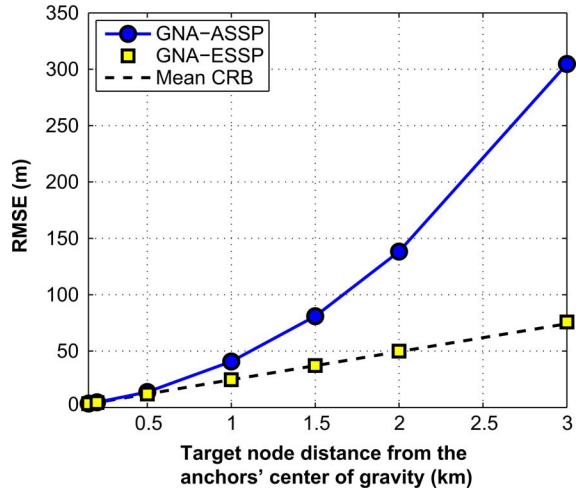

Fig. 6. RMSE vs. the distance of the target node from the anchors' center of gravity, considering DIN.

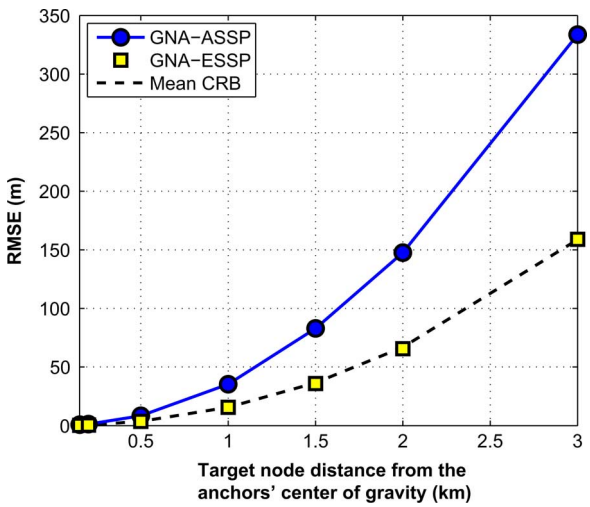

Fig. 7. RMSE vs. the distance of the target node from the anchors' center of gravity, considering DDN.

As is clear from Fig. 4, the performance of the proposed GNA-ESSP constantly improves by increasing the ToF measurement accuracy (decreasing the noise std.), and it falls on top of the mean CRB. On the contrary, the GNA-ASSP does not show any improvement after a given noise std. For large noise stds, both algorithms have the same performance. In that case, the proposed algorithm has no advantage, and the GNA-ASSP is preferred due to its lower complexity.

In Fig. 5, we investigate the performance when the variance of the measurement noise is distance-dependent. To evaluate the algorithm, we introduce a parameter which is the ratio of the expected squared travel time to the noise power:

$$\gamma = \frac{1}{N}\sum_{n=1}^{N}\frac{\mathbb{E}\{t_n^2\}}{\mathbb{E}\{v_n^2\}}. \tag{44}$$

The horizontal axis in Fig. 5 represents γ in dB, and the vertical axis is the RMSE of the location estimate. Here, we assume $l_r = 1000$ m, $\beta = 2$, $K_E = -10$ dB, and $L(f) = 1$ dB/km in (34) and (35) which is valid for frequencies below 20 kHz. In this case, the proposed GNA-ESSP falls on top of the mean CRB while the GNA-ASSP again does not follow the mean CRB after a given γ. This shows that the GNA-ASSP which assumes a constant sound propagation speed is limited and cannot perform as efficient as the proposed algorithm.

In Figs. 6 and 7, we increase the x-coordinate of the reference point around which the target node is located, while the y and z-coordinate of the reference point are $[50, 50]$ as the y and z-coordinate of the anchors' center of gravity. In other words, the horizontal axis in these two figures represents how far the reference point is from the anchor locations. We set $\sigma_n = 1$ ms for the DIN scenario, and for the DDN case, all the parameters are as defined before. From Fig. 6, it can be observed that as the horizontal distance between the target node and the anchor positions increases, the performance of the proposed GNA-ESSP degrades, but it still falls on top of the mean CRB. The reason for this phenomenon can be explained by the non-linear dependency of the ToF measurements to the target location, and the non-equal distribution of the error variance on the estimated location (it depends on the gradient of $\mathbf{f}$ at that point). As a rule of

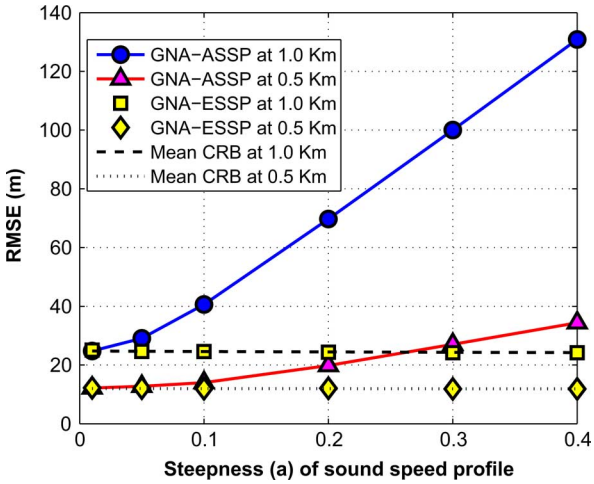

Fig. 8. RMSE vs. SSP steepness.

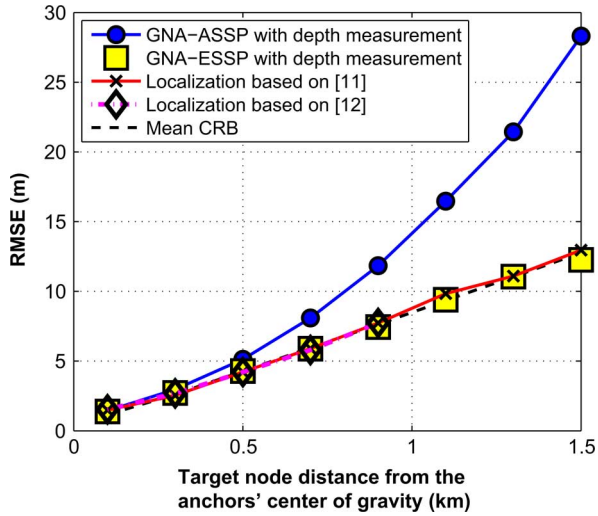

Fig. 9. RMSE vs. the distance of the target node from the anchors' center of gravity, considering DIN, and depth measurement.

thumb, the coordinate which has the lowest corresponding gradient suffers more from the noise. One more thing that can be extracted from this figure is that, although the performance of the proposed algorithm degrades as the distance between the target node and the anchors increases, the GNA-ASSP is affected more by this phenomenon and separates rapidly from the mean CRB as the distance increases.

It can be concluded from Fig. 7 that with a distance-dependent noise variance, not only the non-equal distribution of the error variance on the estimated location affects the performance of the algorithm, but also the increased noise power at larger distances leads to a further degradation.

Fig. 8 depicts the effect of the steepness of the SSP on the performance of the algorithms. Here, we consider a distance-independent noise variance, and we set $\sigma_n = 1$ ms. As can be seen from the figure, with an increase of the steepness of the SSP, the performance of the GNA-ASSP gets worse, but it has no effect on the proposed algorithm. Moreover, this effect is more clear for the case where the target node is further away from the center of gravity of the anchors.

Up to now, we did not consider any depth measurement. In order to compare the proposed localization algorithm with other existing state-of-the-art methods, we assume that the target measures its depth with a measurement noise std. of $\sigma_z = 1$ m and this information can be used in the localization algorithm. In this comparison, the measurement noise of the ToFs is assumed to be DIN with $\sigma_n = 0.5$ ms. In Fig. 9, we compare the performance of the proposed algorithm with the ones introduced in [11] and [12]. These algorithms estimate the horizontal range between two nodes based on the measured ToF and depth. Based on these range estimates, ML localization is performed as in [20].

The work in [11] uses LUTs to compute the mutual horizontal distance between two nodes. For our scenario, two LUTs have to be built. Each LUT has two entries, namely ToF and depth, and one output, namely the horizontal distance. Here, one LUT is responsible to estimate the horizontal distance between the target and the anchors which are located at $z = 0$, and the other LUT estimates the target's horizontal distance from the anchors located at $z = 100$. Each LUT covers a rectangular area of length 2500 m and width 100 m with a resolution of 10 cm. Therefore, each LUT has 25 M points. Fig. 9 shows that the localization algorithm based on [11] performs well, and its performance falls on top of the mean CRB like the proposed algorithm. However, as mentioned before, this algorithm works well only if the SSP of the environment remains constant. Otherwise, the computed values in the LUT are not valid anymore, or are less accurate than expected. The estimation of the horizontal distance in [12] has two phases; first, by measuring the depth and ToF information, the value of k_0 in (3) is computed numerically, and second, by using k_0 and taking the integral w.r.t. the depth of a point on a ray trajectory the value of the horizontal distance can be computed. However, in an inhomogeneous medium, a ray trajectory is not always a monotonic function of the depth, and as a result, whenever a path between two nodes crosses a specific depth more than once, which is quite common, the above algorithm is not valid anymore. This explains why the localization based on [12] works only for regions where the target is close to the anchors. Note though that, this algorithm performs optimal when the ray trajectories to all anchors are a monotonic function of the depth.

For the evaluation of the proposed tracking algorithm, the movement model is chosen to be a random walk with a sampling time step of $T_s = 10$ s. The matrix $\mathbf{\Phi}$ as defined in (38) is then given by

$$\mathbf{\Phi} = \begin{bmatrix} \mathbf{I}_3 & T_s\mathbf{I}_3 \\ \mathbf{0}_{3\times 3} & \mathbf{I}_3 \end{bmatrix},$$

and the process noise covariance matrix, which is assumed to be time-independent and only affecting the velocity, is given by

$$\mathbf{Q} = \begin{bmatrix} \mathbf{0}_{3\times 3} & \mathbf{0}_{3\times 3} \\ \mathbf{0}_{3\times 3} & \mathrm{diag}(\sigma_{\dot{x}}^2, \sigma_{\dot{y}}^2, \sigma_{\dot{z}}^2) \end{bmatrix},$$

where we assume that $\sigma_{\dot{x}} = \sigma_{\dot{y}} = 10^{-2}$, and $\sigma_{\dot{z}} = 10^{-3}$.

For all simulations, we set the initial location guess of the EKF to a point where it is $[30\ \mathrm{m}, 30\ \mathrm{m}, 30\ \mathrm{m}]^T$ away from the actual starting location of the target node. For each run, we

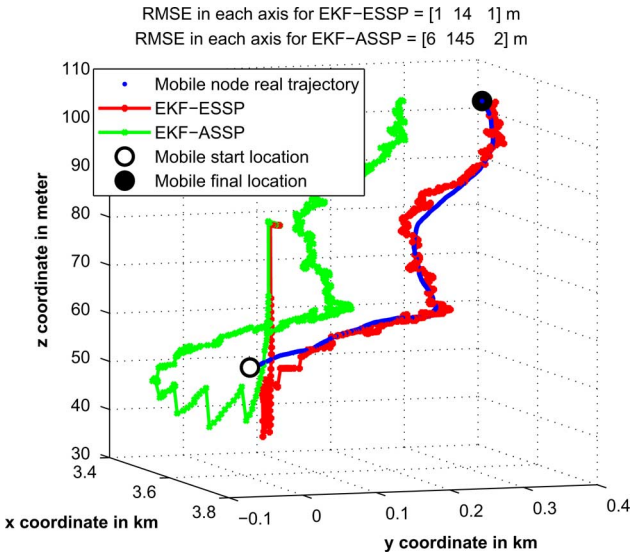

Fig. 10. Tracking comparison.

consider $K = 500$ movement steps, and we compute the positioning root mean squared error (RMSE) between the actual and estimated trajectories at the k-th time instant according to the following formula

$$\mathrm{RMSE}_k = \sqrt{\frac{1}{K-K_1+1}\sum_{k=K_1}^{k=K}\mathbb{E}\left[\left\|\hat{\mathbf{x}}_k-\mathbf{x}_k\right\|^2\right]}, \quad (45)$$

where we try to avoid transient effects by setting K_1 to a large number, e.g., $K_1 = 300$.

As a benchmark for our proposed tracking algorithm (EKF-ESSP), we again show the performance of an ordinary EKF which considers a straight-line wave propagation with a constant sound speed defined as the average sound speed between the depth of the deepest and the shallowest anchors (EKF-ASSP). In the following simulations, we average over 5000 independent Monte Carlo trials and we set $\sigma_t = 1$ ms, $\mathbf{x}_0 = [500\ \mathrm{m}, 50\ \mathrm{m}, 50\ \mathrm{m}]^T$, $\rho = 10$ and $\sigma_z = 1$ m, unless otherwise mentioned.

In Fig. 10, we depict a tracking result example (a single Monte Carlo run) of the proposed EKF-ESSP and the EKF-ASSP algorithm, where the mobile target starts its journey from $[3500\mathrm{m}, 50\mathrm{m}, 50\mathrm{m}]$. It is shown that the proposed algorithm converges well to the real trajectory. However, the EKF-ASSP algorithm always has an offset from the real trajectory, and this offset increases as the mobile target gets further away from the center of gravity of the anchors.

In Fig. 11, we investigate the effect of the measurement noise on the algorithms under consideration. Here, the horizontal axis represents the noise std. on the ToF measurements. As is clear from the figure, the performance of the EKF-ESSP constantly improves when increasing the ToF measurement accuracy (decreasing the noise std.), while the EKF-ASSP does not show any improvement after a given noise std. Further, the performance of the EKF-ASSP gets worse when the distance of the mobile target (in its initial location) from the center of gravity of the anchors increases. For large noise stds, both algorithms have approximately the same performance.

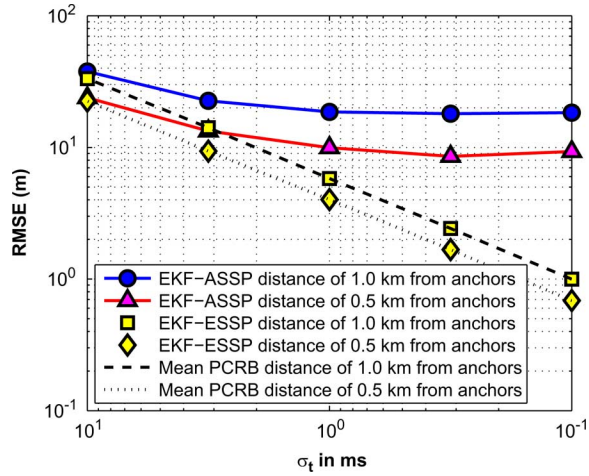

Fig. 11. Effect of the time measurement error.

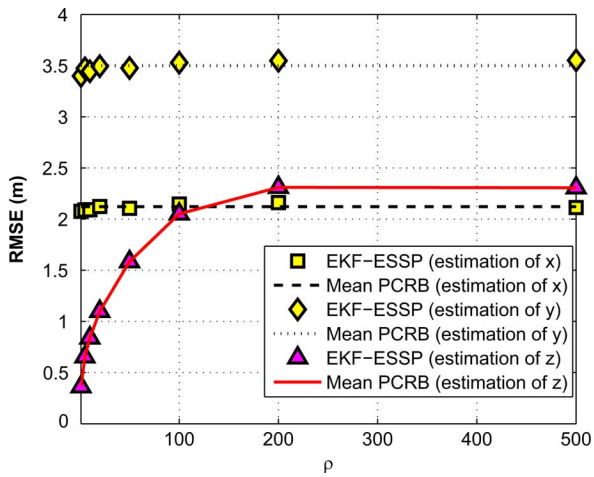

Fig. 12. Effect of the measured depth report on the proposed tracking algorithm.

Fig. 12 shows the effect of the availability of depth measurements on the RMSE performance of the proposed EKF-ESSP algorithm. Increasing the index shown on the horizontal axis (ρ) means that we can less often measure the depth. From the figure, increasing ρ degrades the performance of the EKF-ESSP, although this degradation stops for large values of ρ. This means that the algorithm can work even if it relies only on ToF measurements.

Fig. 13 illustrates the effect of the depth measurement error (denoted by σ_z) on the location estimation errors in each of the axes separately. As can be seen, the depth measurement error mainly affects the location estimates w.r.t. the vertical axis. The lower the depth measurement error, the better the z estimate. On the other hand, increasing the depth measurement error has no effect on the EKF-ESSP after a given value, since at these values, the EKF can acquire a better estimate from the ToFs than from the measured depth, and consequently ignores the depth information by decreasing its corresponding weight in $\breve{\mathbf{K}}$.

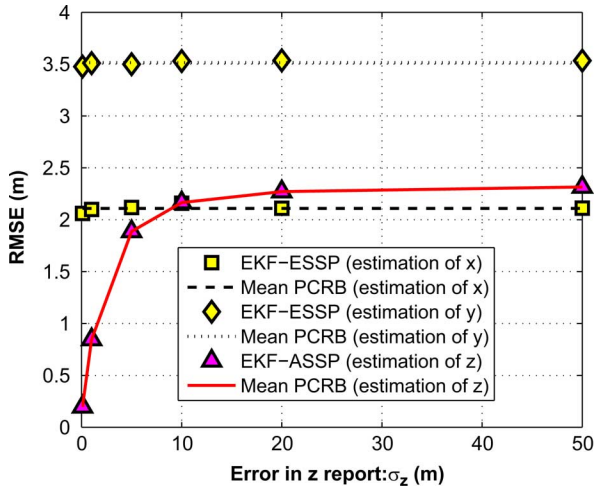

Fig. 13. Effect of the depth measurement error on the proposed tracking algorithm.

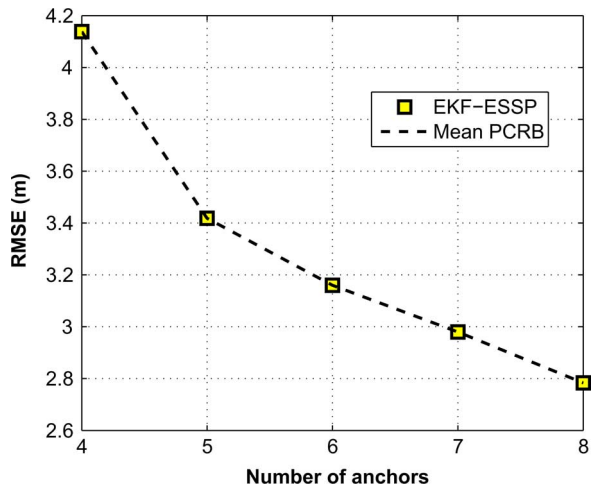

Fig. 14. Effect of the number of anchors on the proposed tracking algorithm.

Finally, Fig. 14 shows the effect of the number of anchors on the performance of the algorithm. The anchors are added one by one and are located on the vertices of the cube as defined before. Although increasing the number of anchors improves the performance of the algorithm slightly, it is not preferred due to the increase in computational complexity.

VI. Conclusions

In this paper, we have considered the problem of target node localization and tracking in an underwater environment with an isogradient SSP. We have shown that the traditional terrestrial approaches for localization which assume a constant sound speed for the whole underwater environment are not so accurate. It is also shown that as the distance between two underwater nodes increases, the straight-line wave propagation model performs worse, since it does not follow the real propagation model. To solve this issue, we relate the ToF between two underwater nodes to their locations for an isogradient SSP, and formulate the localization problem as a time-based problem instead of a range-based one. Then, we use the Gauss-Newton algorithm and the extended Kalman filter with a proper formulation to solve the localization and tracking problem, respectively. It is shown that our proposed algorithms perform better than the algorithms based on a straight-line wave propagation model, especially for large distances. Although an isogradient SSP is not valid for all practical situations, the results can be used as an initial step towards more elaborate SSPs, since any given SSP can be modeled by several isogradient layers. This is a direction of further research.

References

[1] V. Chandrasekhar, W. K. Seah, Y. S. Choo, and H. V. Ee, "Localization in underwater sensor networks: Survey and challenges," in *Proc. 1st ACM Int. Workshop on Underwater Netw. (UWNet '06)*, Sep. 2006, pp. 33–40.

[2] M. Erol-Kantarci, H. T. Mouftah, and S. Oktug, "Localization techniques for underwater acoustic sensor networks," *IEEE Commun. Surv. Tutor.*, vol. 48, no. 12, pp. 152–158, Dec. 2010.

[3] W. K. G. S. H.-P. Tan, R. Diamant, and M. Waldmeyer, "A survey of techniques and challenges in underwater localization," *Elsevier J. Ocean Eng.*, vol. 38, pp. 1663–1676, Oct. 2011.

[4] M. Erol-Kantarci, H. T. Mouftah, and S. Oktug, "A survey of architectures and localization techniques for underwater acoustic sensor networks," *IEEE Commun. Surv. Tutor.*, vol. 13, no. 3, pp. 487–502, 2011.

[5] X. Tan and J. Li, "Cooperative positioning in underwater sensor networks," *IEEE Trans. Signal Process.*, vol. 58, no. 11, pp. 5860–5871, Nov. 2010.

[6] X. Cheng, H. Shu, Q. Liang, and D. H.-C. Du, "Silent positioning in underwater acoustic sensor networks," *IEEE Trans. Veh. Technol.*, vol. 57, no. 3, pp. 1756–1766, May 2008.

[7] M. T. Isik and O. B. Akan, "A three dimensional localization algorithm for underwater acoustic sensor networks," *IEEE Trans. Wireless Commun.*, vol. 8, no. 9, pp. 4457–4463, Sep. 2009.

[8] K. MacKenzie, "Nice-term equation of sound speed in the oceans," *J. Acoust. Soc. Amer.*, vol. 70, pp. 807–812, Sep. 1981.

[9] P. M. Ameer and L. Jacob, "Localization using ray tracing for underwater acoustic sensor networks," *IEEE Commun. Lett.*, vol. 14, no. 10, pp. 930–932, Aug. 2010.

[10] K. Y. Foo and P. Atkins, "A relative-localization algorithm using incomplete pairwise distance measurements for underwater applications," *EURASIP J. Adv. Signal Process.*, Mar. 2010.

[11] G. Casalino, A. Turetta, E. Simetti, and A. Caiti, "RT^2: A real-time ray-tracing method for acoustic distance evaluations among cooperating AUVs," *Proc. OCEANS 2010 IEEE—Sydney*, pp. 1–8, May 2010.

[12] C. R. Berger, S. Zhou, P. Willett, and L. Liu, "Stratification effect compensation for improved underwater acoustic ranging," *IEEE Trans. Signal Process.*, vol. 56, no. 8, pp. 3779–3783, Aug. 2008.

[13] M. B. Porter, "Acoustic models and sonar systems," *IEEE J. Ocean. Eng.*, vol. 18, no. 4, pp. 425–437, Oct. 1993.

[14] P.-M. Lee, B.-H. Jun, J.-H. Li, H. T. Choi, K. Kim, S.-M. Kim, C.-M. Lee, S.-C. Han, B.-M. Gu, S.-R. Lee, H.-S. Chung, and H. S. Choi, "Navigation and control system of a deep-sea unmanned underwater vehicle hemire," in *Proc. OCEANS 2006 -Asia Pacific*, May 2006, pp. 1–8.

[15] N. H. Kussat, C. D. Chadwell, and R. Zimmerman, "Absolute positioning of an autonomous underwater vehicle using GPS and acoustic measurements," *IEEE J. Ocean. Eng.*, vol. 30, no. 1, pp. 153–164, Jan. 2005.

[16] P.-M. Lee, S.-M. Kim, B.-H. Jeon, H. T. Choi, and C.-M. Lee, "Improvement on an inertial-Doppler navigation system of underwater vehicles using a complementary range sonar," in *Proc. Int. Symp. Underwater Technol. UT'04*, Apr. 2004, pp. 133–138.

[17] W. Cheng, A. Thaeler, X. Cheng, F. Liu, X. Lu, and Z. Lu, "Time-synchronization free localization in large scale underwater acoustic sensor networks," in *Proc. 29th IEEE Int. Conf. Distrib. Comput. Syst. ICDCS Workshops '09*, 2009, pp. 80–87.

[18] L. Liu, Y. Xiao, and J. Zhang, "A linear time synchronization algorithm for underwater wireless sensor networks," in *Proc. IEEE Int. Conf. Commun. ICC'09*, Jun. 2009, pp. 1–5.

[19] M. Hahn and J. Rice, "Undersea navigation via a distributed acoustic communication network," in *Proc. Turkish Int. Conf. Acoust.*, Jul. 2005.

[20] S. M. Kay, *Fundamentals of Statistical Signal Processing: Estimation Theory*. Englewood Cliffs, NJ: Prentice-Hall, 1993.
[21] M. Stojanovic and J. Preisig, "Underwater acoustic communication channels: Propagation models and statistical characterization," *IEEE Commun. Mag.*, vol. 47, no. 1, pp. 84–89, Jan. 2009.
[22] P. Tichavsky, C. H. Muravchik, and A. Nehorai, "Posterior Cramér-Rao bounds for discrete-time nonlinear filtering," *IEEE Trans. Signal Process.*, vol. 46, no. 5, pp. 1386–1396, May 1998.
[23] L. Arienzo and M. Longo, "Posterior Cramér-Rao bound for range-based target tracking in sensor networks," in *Proc. IEEE/SP 15th Workshop Statist. Signal Process. SSP '09*, Aug. 2009, pp. 541–544.
[24] Ocean Acoustics Library, Last Access, Oct. 30, 2012 [Online]. Available: http://oalib.hlsresearch.com/Rays/index.html
[25] M. B. Porter, "The BELLHOP Manual and User's Guide: Preliminary Draft," Heat, Light, and Sound Research, Inc., La Jolla, CA, USA, Tech. Rep., 2011 [Online]. Available: http://oalib.hlsresearch.com/Rays/HLS-2010–1.pdf

Hamid Ramezani, was born in Tehran, Iran. He received the B.Sc. degree in electrical engineering from Tehran University, Tehran, Iran, and the M.Sc. degree in telecommunications engineering from the Iran University of Science and Technology, Tehran, Iran, in 2007.

He was working in several companies focusing on the implementations of wireless system standards such as DVB-T and DVB-H. He is currently working towards the Ph.D. degree at the Electrical Engineering Department of Delft University of Technology (TU Delft), Delft, The Netherlands. His current research interests include Underwater acoustic communications and networking.

Hadi Jamali-Rad (S'10) received the B.Sc. degree in electrical engineering from the Iran University of Science and Technology (IUST), Tehran, Iran, in 2007 and the M.Sc. (Hons.) degree in telecommunications engineering from the IUST, in 2010.

He is currently working towards the Ph.D. degree at the Electrical Engineering Department of the Delft University of Technology (TU Delft), Delft, The Netherlands. In 2012, he was a visiting researcher at the Signals, Identification, System Theory and Automation (SISTA) division of Katholieke Universiteit Leuven (KU Leuven), Leuven, Belgium, for which he won a European Erasmus grant. His general interests are in the area of signal processing for communications, wireless networks, and cooperative communications.

Mr. Jamali-Rad has served as reviewer for several IEEE journals and major conferences.

Geert Leus (F'12) received the Electrical Engineering degree and the Ph.D. degree in applied sciences from the Katholieke Universiteit Leuven, Belgium, in 1996 and 2000, respectively.

Currently, he is an Antoni van Leeuwenhoek Full Professor at the Faculty of Electrical Engineering, Mathematics and Computer Science of the Delft University of Technology, Delft, The Netherlands. His research interests are in the area of signal processing for communications.

Dr. Leus received a 2002 IEEE Signal Processing Society Young Author Best Paper Award and a 2005 IEEE Signal processing Society Best Paper Award. He was the Chair of the IEEE Signal Processing for Communications and Networking Technical Committee, and an Associate Editor for the IEEE TRANSACTIONS ON SIGNAL PROCESSING, the IEEE TRANSACTIONS ON WIRELESS COMMUNICATIONS, and the IEEE SIGNAL PROCESSING LETTERS. Currently, he is a member of the IEEE Sensor Array and Multichannel Technical Committee and serves as the Editor-in-Chief of the *EURASIP Journal on Advances in Signal Processing*.